

# Time-Frequency Analysis Using Warped-Based High-Order Phase Modeling

**Cornel Ioana**

ENSIETA, E3I2 Research Centre, 2 rue François Verny, 29806 Brest, France  
Email: ioanaco@ensieta.fr

**André Quinquis**

ENSIETA, E3I2 Research Centre, 2 rue François Verny, 29806 Brest, France  
Email: quinquis@ensieta.fr

Received 7 June 2004; Revised 27 June 2005; Recommended for Publication by Douglas Williams

The high-order ambiguity function (HAF) was introduced for the estimation of polynomial-phase signals (PPS) embedded in noise. Since the HAF is a nonlinear operator, it suffers from noise-masking effects and from the appearance of undesired cross-terms when multicomponents PPS are analyzed. In order to improve the performances of the HAF, the multi-lag HAF concept was proposed. Based on this approach, several advanced methods (e.g., product high-order ambiguity function (PHAF)) have been recently proposed. Nevertheless, performances of these new methods are affected by the error propagation effect which drastically limits the order of the polynomial approximation. This phenomenon acts especially when a high-order polynomial modeling is needed: representation of the digital modulation signals or the acoustic transient signals. This effect is caused by the technique used for polynomial order reduction, common for existing approaches: signal multiplication with the complex conjugated exponentials formed with the estimated coefficients. In this paper, we introduce an alternative method to reduce the polynomial order, based on the successive unitary signal transformation, according to each polynomial order. We will prove that this method reduces considerably the effect of error propagation. Namely, with this order reduction method, the estimation error at a given order will depend only on the performances of the estimation method.

**Keywords and phrases:** high-order ambiguity function, polynomial phase signal, warping operator.

## 1. INTRODUCTION

It is well known that there is no distribution of the Cohen's class which might produce the complete concentration along the instantaneous frequency law (IFL) when this one is a nonlinear function of time. Matching these types of signals requires a new joint distribution with different instantaneous frequency and group delay localization properties. One of the most known techniques [5] is the unitary similarity transformation. Using this concept it is possible to construct, via the warping operators, distributions to match almost any one-to-one group delay or instantaneous frequency characteristics. More precisely, by warping the analyzed signal according to the nature of its IFL, it is possible to "linearize" the time-frequency content of the considered signal. Nevertheless, this concept requires the knowledge of the nonlinearity type, necessary to design the warping operators.

An alternative way to better match the nonlinear time-frequency behavior of the analytical signals (i.e., whose phase can be expressed as a finite series expansion) is to use the high-order time-frequency distributions. Since the

polynomial phase signal constitutes a good model in a variety of applications (e.g., radar imagery, mobile communication systems [2], etc.), the high-order time-frequency methods have been developed.

Nowadays, these two research fields—generalization of the classical time-frequency distribution and the data modeling via the polynomial phase signal concept—have received considerable attention in the literature [1, 2, 3, 4] and the references therein. It is primarily due to the number of possible applications, especially for signals having a nonlinear time-frequency behavior: underwater signal processing, digital modulations, radar signals, and so forth. Mathematically, a noiseless polynomial phase signal can be modeled as

$$s(t) = A \exp \{j\phi(t)\} = A \exp \left[ j \sum_{k=0}^N a_k t^k \right], \quad (1)$$

where  $N$  is the polynomial order of the phase  $\phi(t)$ ,  $\{a_k\}_{k=1,\dots,N}$  are the polynomial coefficients, and  $A$  is the signal amplitude.

One of the first approaches to estimate the parameters of the PPSs is high-order ambiguity function (HAF) [1] which provides good results for high signal-to-noise ratio. The underlying idea is the transformation of the signal in a nonlinear way in order to obtain a tone whose frequency is directly related to the corresponding polynomial coefficient. The estimation accuracy of this method has been devised in [6]. Nevertheless, since the HAF is a nonlinear method, it suffers from three basic problems: (1) noise-masking effects for low signal-to-noise ratios (SNR), (2) cross-terms in the presence of multicomponent PPSs (mc-PPSs), and (3) propagation of the approximation error from an order to other.

Recently, different methods have been proposed in order to eliminate the first two limitations. The key point is to use the multilag concept in the HAF computing procedure [2]: using a set of distinct lags, it is possible to eliminate the cross-terms and to improve the noise robustness. Moreover, multiplying the HAFs obtained for some lag sets (Product HAF—PHAF), the performances related to noise robustness and cross-terms effect are considerably improved with respect to multilag HAF (mlHAF) [2].

Since the Wigner-Ville distribution constitutes the classical tool for chirp signal processing, a natural way to estimate the nonlinear IFL of a PPS is based on the polynomial Wigner-Ville distribution (PWVD) introduced in [3]. The concept of this method is based on the creation, in the time-frequency domain, of a delta function around the IFL of the signal. Later, the L-Wigner distribution is introduced in order to provide a good concentration around the IFL, preserving the interesting properties of the Wigner-Ville distribution. These two concepts have been generalized in [7] starting with the definition of the high-order polynomial derivatives decompositions in terms of a linear combination of the translated version of the polynomial. The generalized ambiguity function and the generalized Wigner distribution were also proposed.

An alternative way for the estimation of the PPS parameters is the use of the Bayesian-like procedure. An interesting approach, based on Markov chain Monte Carlo methods for estimation of the a posteriori densities of the polynomial parameters, is proposed in [8]. The aim of this work deals with a direct estimation of the polynomial coefficients, contrary to the works previously mentioned.

In practical application, the use of the polynomial modeling procedures requires to set up some parameters. Namely, for the high-order ambiguity function computation, a lag set has to be defined. This problem has been the subject of several works. In [5], the authors proposed a criterion based on the minimization of estimation variances. This work has been generalized in [2] in the case of PHAF. Alternatively, by using two coprime lag values, we can improve both the estimation accuracy and the evaluation of signal component number [9].

In spite of the improved performances of these approaches, effect of propagation error remains a serious drawback when trying to estimate a high nonlinear IFL (underwater transitory signals, digital modulations, etc.). More specifically, this effect reduces drastically the approximation order

for which an accurate estimation of the IFL is furnished. This effect, firstly analyzed in [5], is caused by the polynomial order compensation, currently performed by multiplying the signal with the reference  $\exp\{-j\hat{a}_k t^k\}$ , where  $\hat{a}_k$  is the estimation of  $k$ th-order coefficient.

Thence, one way to reduce the error propagation effect is to use a new method for polynomial order reduction. The method proposed in this paper is based on the polynomial order reduction by warping successively the analyzed signal.

Conventionally, a warping operator is designed to “linearize” the time-frequency behavior of the analyzed signal. For time-frequency analysis purposes, this “linearization” is taken into account by applying a classical time-frequency distribution (e.g., Wigner-Ville Distribution—WVD) on the warped signal. In this paper, we propose an alternative use of the warping operator concept.

We design a warping operator whose effect will be the polynomial order reduction. In the context of the polynomial phase modeling, this effect will be taken into account by computing the mlHAF of the warped signal. Furthermore, through several examples and performance analysis, we will prove that this method reduces considerably the effect of error propagation.

This paper is organized as follows. In Section 2, the concept of the mlHAF is presented. Section 3 describes the major limitation of the mlHAF, related to the error propagation effect. The main tools introduced in this paper—“unitary operators”—will be shortly explained in Section 4. Furthermore, a new method for order compensation will be depicted in Section 5. Several signal processing examples will be presented in Section 6. Section 7 presents some remarks and ideas for future works.

## 2. MULTILAG HIGH-ORDER AMBIGUITY FUNCTION

The high-order ambiguity function (HAF) was originally designed for estimation of a single component, constant amplitude PPS, given by the relation (1). The HAF is defined as the Fourier transform of the high-order instantaneous moments (HIM) given, for a signal  $s(t)$ , by the following relation:

$$\text{HIM}_K [s(t); \tau] \triangleq \prod_{q=0}^{K-1} [s^{(*q)}(t - q\tau)]^{\binom{K-1}{q}}, \quad (2)$$

where  $K$  is the HIM order,  $\tau$  is the lag, and  $(*q)$  is an operator defined as

$$s^{(*q)}(t) = \begin{cases} s(t), & \text{if } q \text{ is even,} \\ s^*(t), & \text{if } q \text{ is odd,} \end{cases} \quad (3)$$

where  $q$  is the number of conjugate operator “\*” applications. From the computational point of view, the main property of the HIM [1] states that the  $K$ th-order HIM can be computed as the 2nd-order HIM of the  $(K-1)$ th-order HIM:

$$\text{HIM}_K [s(t); \tau] = \text{HIM}_2 [\text{HIM}_{K-1} [s(t); \tau]; \tau]. \quad (4)$$

Another remarkable property, which makes HIM an attractive tool in the polynomial phase modeling context, is that the  $N$ th-order HIM of a PPS given in (1) is reduced to a constant amplitude harmonic with amplitude  $A^{2^{N-2}}$ , frequency  $\tilde{\omega}_N$ , and phase  $\tilde{\phi}_N$  [1]:

$$\text{HIM}_N [s(t); \tau] = A^{2^{N-1}} \exp j(\tilde{\omega}_N \cdot t + \tilde{\phi}_N), \quad (5)$$

where

$$\begin{aligned} \tilde{\omega}_N &= N! \tau^{N-1} a_N, \\ \tilde{\phi}_N &= (N-1)! \tau^{N-1} a_{N-1} - 0.5N!(N-1)\tau^N a_N. \end{aligned} \quad (6)$$

A natural idea to take advantage of this property is to compute the Fourier transform of  $N$ th-order HIM, which leads to the HAF definition [1]:

$$\text{HAF}_N [s; \omega, \tau] = \int_{-\infty}^{\infty} \text{HIM}_N [s(t); \tau] e^{-j\omega t} dt. \quad (7)$$

Obviously, taking into consideration the relation (5), the  $N$ th-order HAF of the signal given in (1) peaks at the frequency  $\tilde{\omega}_N$ . This property gives a practical method for polynomial coefficients estimation [1]. Starting with the highest-order coefficient  $a_N$ , the maximum of the HAF is evaluated at each order. The  $N$ th-order polynomial coefficient is estimated via

$$\hat{a}_N = \frac{1}{N! \tau^{N-1}} \arg \max_{\omega} \{ |\text{HAF}_N (s; \omega, \tau)| \}. \quad (8)$$

Using this estimation, the effect of the phase term of the higher order is removed:

$$s^{(N-1)}(t) = s(t) \cdot e^{-j\hat{a}_N t^N}. \quad (9)$$

Once the  $N$ th-order is reduced, the  $(N-1)$ th-order HAF is computed. The coefficient  $a_{N-1}$  is also estimated thanks to relation (8). The algorithm is iterated through the inferior orders until all polynomial coefficients are estimated.

As it was illustrated in [1, 2], the classical procedure for polynomial phase modeling, based on HAF method, is practically affected by some limitations regarding the noise robustness and the cross-terms presence. To overcome these problems, the multilag HAF (mlHAF) concept has been initially proposed in [2]. In fact, the mlHAF is based on the generalization of the high-order instantaneous moment HIM [2], based on the property expressed in relation (4):

$$\begin{aligned} \text{mlHIM}_N [s(t); \tau_{N-1}] \\ = \text{mlHIM}_{N-1} [s(t + \tau_{N-1}); \tau_{N-2}] \\ \times \text{mlHIM}_{N-1}^* [s(t - \tau_{N-1}); \tau_{N-2}], \end{aligned} \quad (10)$$

where  $\tau_N = (\tau_1, \tau_2, \dots, \tau_N)$  is the set of lags. Applying the Fourier transform, exactly as for the case of the HAF (7), we obtain the mlHAF of the signal  $s(t)$ :

$$\text{mlHAF}_N [s; \omega, \tau_N] = \int_{-\infty}^{\infty} \text{mlHIM}_N [s(t); \tau_N] e^{-j\omega t} dt. \quad (11)$$

In practical applications, the choice of the lags set  $(\tau_1, \tau_2, \dots, \tau_N)$  is often difficult to do. One possible solution, proposed in [2], is  $\prod_{i=1}^{N-1} \tau_i = \text{const} = \tau^{N-1}$ . Based on the resolution capability criterion [2], it can be shown that  $\tau = L/N$  ( $L$ -signal length) represents the optimal choice.

Using the mlHAF computed for a lag set provided in this manner, the polynomial coefficients are estimated with relation (8). In [2], the performances of the mlHAF-based procedure are proved. Nevertheless, there are still some limitations related to the noise reduction and cross-terms. To surmount these limitations, Barbarossa et al. [2] introduced the product HAF (PHAF). The mlHAFs computed, via relation (11), for different lag sets:

$$\mathbf{T} = \left\{ \tau_{N-1}^{(l)} \right\}_{1 \leq l \leq P}; \quad \tau_{N-1}^{(l)} = \{ \tau_i \}_{1 \leq i \leq N-1}, \quad (12)$$

are multiplied, obtaining in this way a robust method and a cross-term free representation:

$$\text{PHAF}(f; \mathbf{T}) = \prod_{l=1}^P \text{mlHAF}_N \left[ s; \frac{\prod_{i=1}^{N-1} \tau_i^{(l)}}{\prod_{i=1}^{N-1} \tau_i^{(1)}} f, \tau_{N-1}^{(l)} \right], \quad (13)$$

where  $P$  is the number of the lags set used at each order.

The next example illustrates the PHAF superiority (Figure 1b) with respect to mlHAF-based procedure. We consider, as a test signal, a two component 3rd-order PPS:

$$\begin{aligned} s(t) &= \exp \left[ j2\pi \left( 0.25 \cdot t - \frac{0.05}{L} t^2 + \frac{0.28}{L^2} t^3 \right) \right] \\ &+ \exp \left[ j2\pi \left( 0.45 \cdot t + \frac{0.15}{L} t^2 - \frac{0.12}{L^2} t^3 \right) \right] \quad (L = 306) \end{aligned} \quad (14)$$

embedded in an additive white Gaussian noise (SNR = 10 dB).

In order to illustrate the differences between mlHAF and PHAF, Figure 1 is structured in two parts associated with both methods: Figure 1a—mlHAF and Figure 1b—PHAF. Each part contains six subplots organized as follows: each subplot row is associated to a signal component and, inside the row, each subplot corresponds to mlHAF estimation of order 3 (right subplot) to 1 (left subplot). The  $x$ -axis of each subplot corresponds to the frequency and the  $y$ -axis to magnitude. Values of estimated coefficients are also given. The same rule is used throughout this paper.

As illustrated in this figure, in the mlHAF case, the reduced number of lags affects the IFL estimation quality (Figure 1a). This result can be explained by the spurious spectral peaks which appear in the mlHAF spectra (Figure 1a—the subplots associated to each component at a given order). Consequently, the estimation of the polynomial coefficients becomes poor especially for lower orders.

On the other hand, the PHAF solves the noise robustness and multicomponent estimation problems, providing also a correct IFL estimation (Figure 1b). The PHAF-based estimated values of the polynomial coefficients are close to the real ones. This is also illustrated in Figure 1b by a correct localization of each PHAF maximum, corresponding to

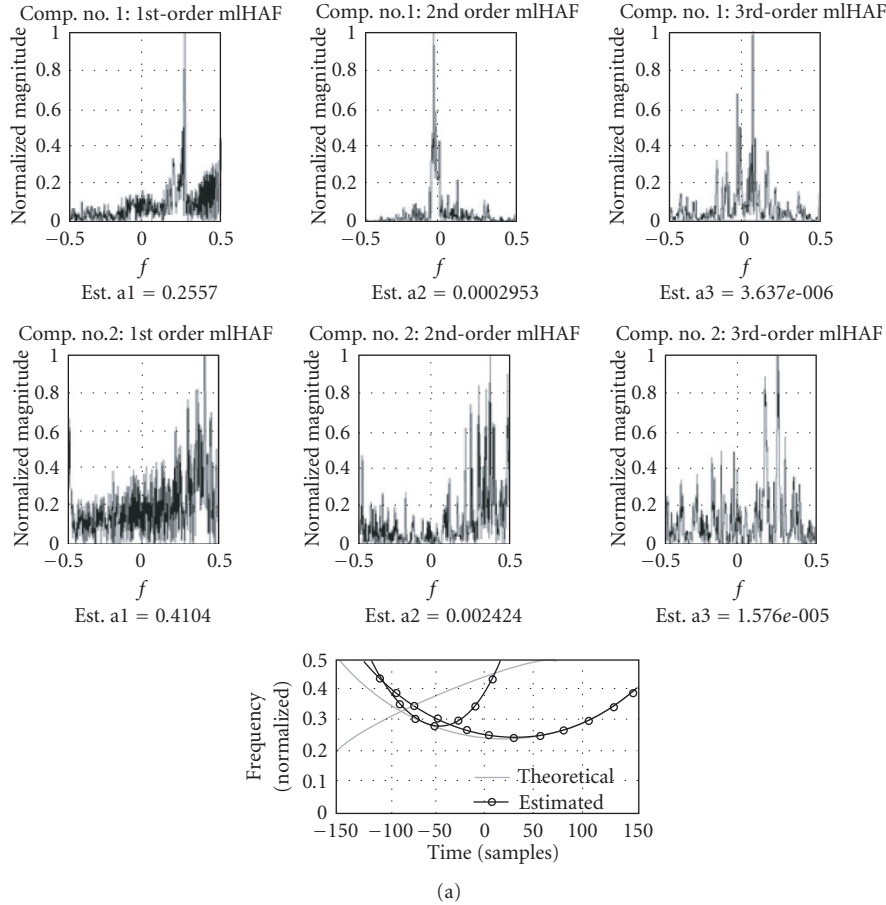


FIGURE 1: (a) mlHAF-based procedure versus (b) PHAF-based procedure.

the associated polynomial coefficient. Namely, as illustrated by the subplots associated to each polynomial order, the coefficients belonging to each signal component are accurately estimated.

Still, this “nice” result was obtained for a signal having a smooth time-frequency behavior. If this condition is not verified (the signals whose phases are modeled by a high polynomial order, such as underwater transient signals [17]), a limitation that cannot be neglected acts. It is related to the error propagation effect evaluated in the next section.

### 3. ERROR PROPAGATION EFFECT IN POLYNOMIAL PHASE MODELING

The approach presented in this paper constitutes a particularization of the results obtained in [5]. In this section, we will evaluate the dependence expression of the errors for two consecutive orders and for a particular value of the lag. The purpose is to provide a suggestive overview on the error propagation effect.

We consider the signal given in (1) and we denote with  $\hat{a}_N$  the estimation of the  $N$ th-order polynomial coefficient. In real applications [1], since the mlHAF-based polynomial coefficients evaluation involves a spectral estimation step (8) of a discrete sequence, the estimated value differs from the theoretic one by  $\varepsilon_N = a_N - \hat{a}_N$ . This quantity denotes the

approximation error and it is directly related to the number of Fourier points and the SNR [2]. Using this estimate, we remove the  $N$ th-order coefficient via (9). Consequently, the corresponding  $(N - 1)$ th-order PPS becomes

$$s^{(N-1)}(t) = A e^{j(\sum_{k=0}^{N-1} a_k t^k + (a_N - \hat{a}_N) t^N)} = A e^{j \sum_{k=0}^{N-1} a_k t^k} \cdot e^{j \varepsilon_N t^N}. \quad (15)$$

For simplicity reasons we consider  $A = 1$ . With relation (2) and the notation  $\tilde{s}(t) = e^{j \sum_{k=0}^{N-1} a_k t^k}$ , the  $(N - 1)$ th-order HIM is expressed as

$$\begin{aligned} & \text{HIM}_{N-1} [s^{(N-1)}(t); \tau] \\ &= \left\{ \prod_{q=0}^{N-1} [\tilde{s}^{(*q)}(t - q\tau)] \right\}^{(N-1)} \left\{ \prod_{q=0}^{N-1} [e^{j \varepsilon_N (-1)^q (t - q\tau)^N}] \right\}^{(N-1)}. \end{aligned} \quad (16)$$

According to the property stated by the relation (5), we can write

$$\text{HIM}_{N-1} [s^{(N-1)}(t); \tau] = e^{j[(N-1)! \tau^{N-2} \hat{a}_{N-1} t + \hat{\phi}_{N-1}]}, \quad (17)$$

where  $\hat{\phi}_{N-1} = (N - 2)! \tau^{N-2} a_{N-2} - 0.5(N - 1)!(N - 2) \tau^{N-1} \hat{a}_{N-1}$  as obtained with relation (6).

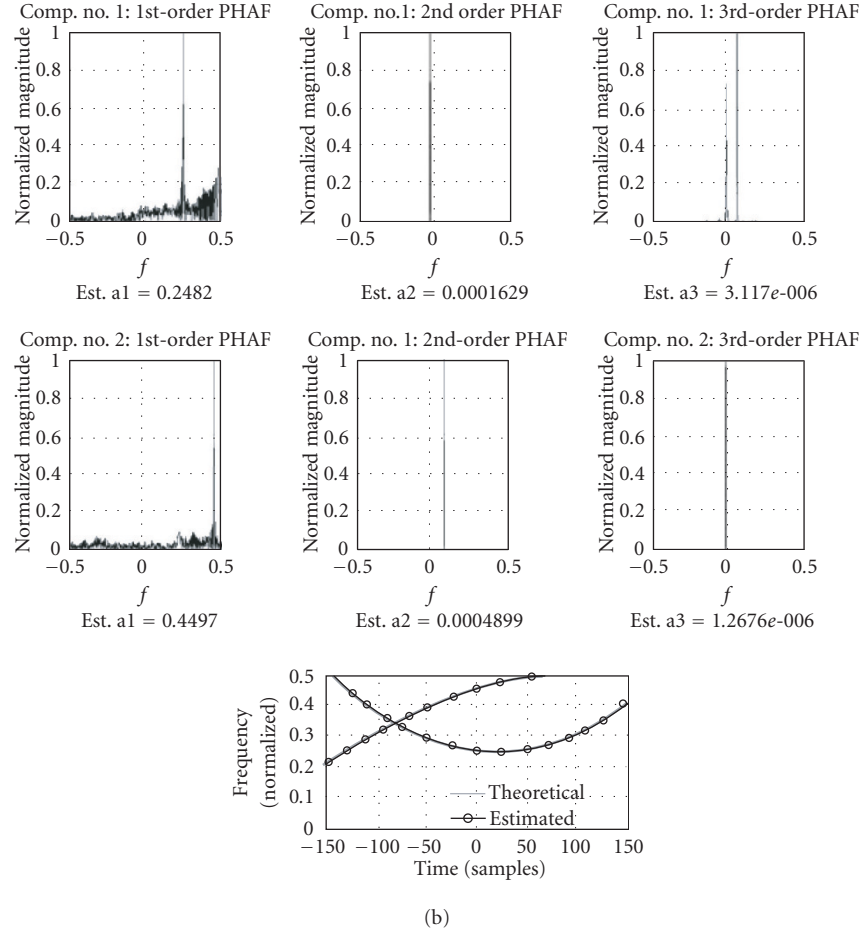


FIGURE 1: Continued.

This expression is the consequence of the main HAF property previously presented: the  $(N - 1)$ th-order HIM of a given signal is a sinusoid with an angular frequency related, via (6), to the  $(N - 1)$ th-order polynomial coefficient. Nevertheless, due to the measurement error which occurs for the  $N$ th order, the coefficient  $\hat{a}_{N-1}$  is not equal to the theoretical  $(N - 1)$ th-order polynomial coefficient,  $a_{N-1}$ , of signal  $s$ . To find the relation between the errors at two successive orders,  $N$  and  $(N - 1)$ , we evaluate the two products which appear in relation (16).

With property (5) and observing that  $\tilde{s}(t) = e^{j\sum_{k=0}^{N-1} a_k t^k}$  is an  $(N - 1)$ th-order PPS, which could be ideally obtained if  $\varepsilon_N = 0$ , the first product becomes

$$\begin{aligned} \text{HIM}_{N-1}[\tilde{s}(t); \tau] &= \prod_{q=0}^{N-1} [\tilde{s}^{*(q)}(t - q\tau)] \binom{N-1}{q} \\ &= e^{j[(N-1)!\tau^{N-2}a_{N-1}t + \phi_{N-1}]}, \end{aligned} \quad (18)$$

where  $\phi_{N-1}$  can be expressed, thanks to (6), as follows:

$$\phi_{N-1} = (N - 2)! \tau^{N-2} a_{N-2} - 0.5(N - 1)!(N - 2)\tau^{N-1} a_{N-1}. \quad (19)$$

The second term of the product in (16) can be written, applying the Newton's binomial formula to the term  $(t - q\tau)^N$ , as

$$\begin{aligned} &\prod_{q=0}^{N-1} [e^{j\varepsilon_N(-1)^q(t-q\tau)^N}] \binom{N-1}{q} \\ &= \exp \left[ j\varepsilon_N \sum_{q=0}^{N-1} (-1)^q \binom{N-1}{q} (t - q\tau)^N \right] \\ &= \exp \left[ j\varepsilon_N \sum_{q=0}^{N-1} (-1)^q \binom{N-1}{q} \sum_{i=0}^N \binom{N}{i} t^i (-q)^{N-i} \tau^{N-i} \right]. \end{aligned} \quad (20)$$

Since the peak corresponding to a polynomial coefficient is extracted by the HAF (i.e., Fourier transform of the HIM), at a given order, in the expression of the corresponding HIM, we always look for the term which weights  $t$ . Consequently, from (20), we retain the term

$$\exp \left[ jN\varepsilon_N \tau^{N-1} \sum_{q=0}^{N-1} (-1)^q \binom{N-1}{q} (-q)^{N-1} \right] t. \quad (21)$$

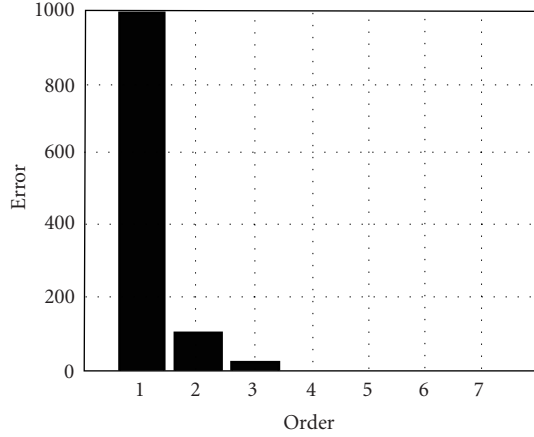


FIGURE 2: Error propagation effect ( $N = 8, L = 10$ ).

Introducing (17), (18), and (21) in (16) and identifying the terms weighting  $t$ , we obtain the relation between the estimation of the  $(N - 1)$ th-order polynomial coefficient ( $\hat{a}_N$ ), the theoretical  $(N - 1)$ th-order polynomial coefficient ( $a_N$ ), and the error at order  $N$  ( $\varepsilon_N$ ):

$$(N - 1)! \tau^{N-2} \hat{a}_{N-1} = (N-1)! \tau^{N-2} a_{N-1} + N \varepsilon_N \tau^{N-1} \sum_{q=0}^{N-1} (-1)^q \binom{N-1}{q} (-q)^{N-1}. \quad (22)$$

With the notation  $\varepsilon_{N-1} = \hat{a}_{N-1} - a_{N-1}$ , (22) becomes

$$\varepsilon_{N-1} = \frac{N \varepsilon_N \tau}{(N-1)!} \underbrace{\sum_{q=0}^{N-1} (-1)^q \binom{N-1}{q} (-q)^{N-1}}_{S_q}. \quad (23)$$

In [12], it is shown that the summation  $S_q$  is  $(N - 1)!$ . With this result, the dependence between the errors existing for two successive polynomial orders is

$$\varepsilon_{N-1} = N \varepsilon_N \tau \quad (24)$$

and, using the optimal value of the lag previously defined, that is,  $\tau = L/N$ , we get

$$\varepsilon_{N-1} = L \varepsilon_N. \quad (25)$$

This relation shows that the error existing at a given order is transmitted at the inferior order by multiplication of  $L$ —the number of samples of the signal. Figure 2 illustrates this dependence for  $L = 10$  samples.

From this figure, it can be observed that even if the measurement error for the highest order is insignificant, its effect through the lower orders becomes deeply disturbing.

On the other hand, we remark that this effect becomes “visible” after the polynomial estimation at some orders. It explains why the error propagation effect does not affect

the polynomial estimation when a small approximation order is required (3 or 4). Anyway, there are many situations which impose a high approximation order: digital modulations, transitory signals, and so forth. One example is given in Figure 3 where we process, via the PHAF-based phase modeling method, a sixth-order PPS whose analytical form is given by

$$s(t) = \exp [j2\pi(0.17 \cdot t - 9.7 \cdot 10^{-4} \cdot t^2 - 2.35 \cdot 10^{-7} \cdot t^3 + 3.8 \cdot 10^{-8} \cdot t^4 + 2.8 \cdot 10^{-10} \cdot t^5 - 3.29 \cdot 10^{-13} \cdot t^6)]. \quad (26)$$

The theoretical IFL is plotted in Figure 3b. Note that the SNR is about 30 dB.

The PHAF-based estimation procedure was applied, starting with order 6. The successive PHAF spectra are depicted in Figure 3a. The values of the estimated coefficients are depicted in the Table 1. They are obtained via the relation  $\hat{a}_N = 1/N! \tau^{N-1} \arg \max_f |\text{PHAF}_N(f; T)|$ , where  $\tau = L/N$  ( $L$  is the signal length) and  $\hat{a}_N = \arg \max_f |\text{PHAF}_N(f; T)|$  is the normalized frequency coordinate associated to the most energetic  $N$ th-order PHAF peak. This value ranges between  $-0.5$  and  $0.5$  and, for the considered example, they are given in Table 1. Dividing such value by  $N! \tau^{N-1}$  explains the very small values of the polynomial coefficients at the high orders.

For higher orders (6, 5), PHAF performs quite well: the propagation error is insignificant, but its effect is accumulated and it becomes disturbing for lower orders (down to 5). The error propagation is materialized by a more accentuated presence of spurious peaks with order decreasing (Figure 3a). The estimated coefficients (Table 1) are different in comparison with the real coefficients given in (26). Consequently, the estimation of the polynomial coefficient is not correct (Figure 3b); the evaluated IFL does not match the correct time-frequency behavior of the analyzed PPS.

This example illustrates the error propagation effect that was analyzed in this section. We have shown that this effect is caused by the classical phase removing the step illustrated in (15).

In the Section 5 we propose an alternative method to reduce the polynomial order. This method is based on the warping technique concept briefly presented in the next section.

#### 4. WARPING OPERATOR PRINCIPLE

Unitary similarity transformations furnish a simple powerful tool for generating new classes of joint distributions based on concepts different from time, frequency, and scale [10]. These new signal representations focus on the critical characteristics of large classes of signals, and, hence, prove useful for representing and processing signals that are not well matched by current techniques. Actually, it is possible to construct (via unitary transformations) distributions to match almost any one-to-one group delay or instantaneous frequency characteristics. One of the most used unitary transforms is the *axis*

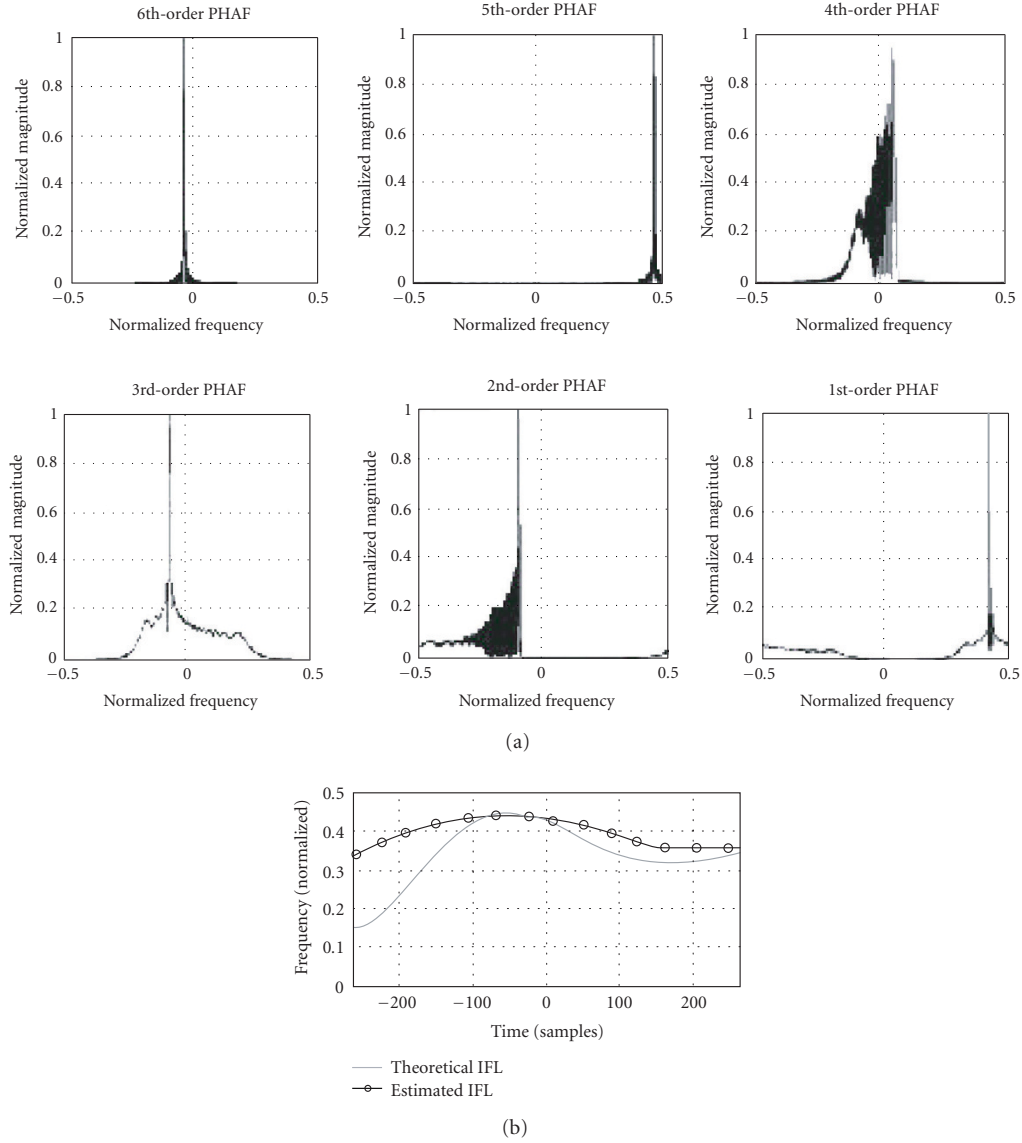


FIGURE 3: PHAF-based phase modeling of a sixth-order PPS. (a) Classical phase removing. (b) Theoretical and estimated IFL.

TABLE 1: Polynomial coefficients estimated by PHAF.

	$\hat{\alpha}_1$	$\hat{\alpha}_2$	$\hat{\alpha}_3$	$\hat{\alpha}_4$	$\hat{\alpha}_5$	$\hat{\alpha}_6$
Values	0.425	-0.112	-0.0961	0.084	0.4714	-0.0817
	$\hat{a}_1$	$\hat{a}_2$	$\hat{a}_3$	$\hat{a}_4$	$\hat{a}_5$	$\hat{a}_6$
Values	0.425	$-3.634 \cdot 10^{-4}$	$-1.54 \cdot 10^{-6}$	$7.82 \cdot 10^{-9}$	$2.8 \cdot 10^{-10}$	$-3.29 \cdot 10^{-13}$

transformation [10], defined for a signal  $s(t)$  as an operator  $\mathbf{U}$  on  $L^2(\mathfrak{R})$ , whose effect is given by

$$(\mathbf{U}s)(x) = |\dot{w}(x)|^{1/2} s[w(x)], \quad (27)$$

where  $w$  is a smooth, one-to-one function, including a large subclass of unitary transformations [10]. The term  $\dot{w}(x)$  denotes the first-order derivative of the function  $w$ . The functions  $w(x) = e^x$  and  $w(x) = |x|^k \text{sgn}(x)$ ,  $k \neq 0$ , provide

examples of useful warpings [13, 14]. Generally, these functions are chosen to ensure the “linearization” of the signal time-frequency behavior. So, for a signal expressed as

$$s(t) = e^{j2\pi(f_0 t + \beta m(t))}, \quad (28)$$

where  $m(t)$  is the frequency modulation law and  $\beta$  the rate modulation, the associated warping function is given by [10]

$$w(t) = m^{-1}(t). \quad (29)$$

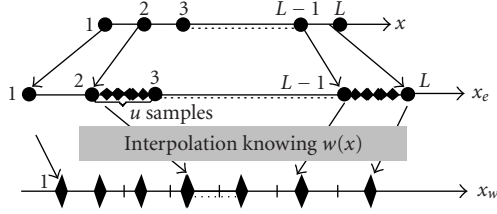


FIGURE 4: Warping technique: implementation scheme.

As shown in [10], the application of this operator produces the linearization of the time-frequency content.

Practically, the application of a warping operator is similar to the coordinate changing stated by the warping law. In [17] an efficient implementation scheme is proposed: the warping operator application effect is done according to stages depicted in Figure 4.

Firstly, the original axis of the signal, whose length is  $L$ , is oversampled with a rate  $u$ . The new finest sampling grid leads to a more accurate evaluation of the new coordinates [17]. This operation is done in the second stage. Using the discrete version of the warping function,  $w(x)$ , we evaluate the new coordinates. Since the warping function gives generally a noninteger number, an interpolation procedure will be used to generate the appropriate integer coordinates. Then, the warped signal is generated by resampling the signal for these new coordinates.

Furthermore, the linearization of the time-frequency content is taken into account by computing the Wigner-Ville distribution (WVD) of the warped signal [17]:

$$\text{WVD}_{U_s}(\tilde{t}, \tilde{f}) = \int (\mathbf{U}_s)\left(\tilde{t} + \frac{\tau}{2}\right) (\mathbf{U}_s)^*\left(\tilde{t} - \frac{\tau}{2}\right) e^{-j2\pi\tilde{f}\tau} d\tau. \quad (30)$$

The new time-frequency coordinates are related to the standard ones via [16]

$$\tilde{t} = w^{-1}(t), \quad \tilde{f} = f\dot{w}(w^{-1}(t)), \quad (31)$$

where  $w^{-1}$  is the inverse function of  $w(t)$ . We note that this relation is available in the case of time warping operators. An alternative formula can be devised for the frequency warping operators [16, 17].

The following example illustrates the property of warping operators related to the linearization of the time-frequency behavior. For a signal given by

$$s(t) = e^{j2\pi(0.38t - 0.02t^{1.3})}, \quad (32)$$

the associated warping operator can be defined as [15]

$$\begin{aligned} \mathbf{U}_{1/k} : w(t) &= t^{1/k}, \quad k = 1.3, \\ \dot{w}(t) &= \frac{1}{k} t^{(1/k)-1}. \end{aligned} \quad (33)$$

According to this operator, the mathematical expression of the warped signal is

$$(\mathbf{U}_{1/k}s)(t) = e^{j2\pi(0.38t^{1/1.3} - 0.02t)}. \quad (34)$$

The evaluation of the WVD of this signal in original time and frequency coordinates leads to a complicate time-frequency behavior as indicated in Figure 5.

Obviously, the nonlinear time-frequency content of the original signal (Figure 5a) is transformed, via WVD computed for conventional time-frequency coordinates, in a new nonlinear time-frequency form.

Therefore, in order to take advantage of the warped form of the oversampled signal, the WVD must be computed, via (30), in the new time and frequency coordinates associated to the warping operators. Thanks to (31) for the warping function devised in (33), the new time-frequency coordinates are written as

$$\begin{aligned} \tilde{t} &= w^{-1}(t) = t^k, \\ \tilde{f} &= f\dot{w}(t^k) = f\frac{1}{k}(t^k)^{1/k-1} = \frac{f}{k}t^{1-k} \end{aligned} \quad (35)$$

and, for  $k = 1.3$ ,

$$\tilde{t} = t^{1.3}, \quad \tilde{f} = \frac{f}{1.3}t^{-0.3}. \quad (36)$$

As indicated in Figure 4, in order to obtain a more accurate evaluation of the warped time axis, an oversampling procedure is applied to the original signal [17]. The oversampled signal,  $s_u$ , represented in a finer time axis coordinates,  $t_u$ , is warped via (33). The WVD of the warped version of the oversampled signal  $((\mathbf{U}_{1/k}s_u)(t_u))$ ,  $u = 10$  is plotted in Figure 6b. Comparing this figure with Figure 5b, we remark that the time-frequency content of  $((\mathbf{U}_{1/k}s_u)(t_u))$  is less nonlinear than the one of the  $(\mathbf{U}_{1/k}s)(t)$  (Figure 5b). This is related to the advantage of the warping application on the oversampled signal.

As we can see in Figure 6a, due to the term  $0.38t_u^{1/1.3}$  of the warped signal (34), nonlinearity is still visible in the interval of  $0 \div 100$  samples. That is, even if the signal is warped after oversampling, this term is again visible. This nonlinearity is eliminated by computing, using (30), the WVD for new time and frequency coordinates depicted in (36). As illustrated in Figure 6b, the result is a linear time-frequency structure.

This example illustrates the capability of the warping operator concept to linearize the time-frequency content of a signal. As theoretically shown in [17], two steps are involved. Firstly, the signal is warped according to its modulation nature. Secondly, the WVD of warped signal is evaluated, using the new time and frequency coordinates.

Both theoretical and practical issues, previously presented, suppose some knowledge on the time-frequency nature of the signal (the warping function  $w(t)$  has to be known). Nevertheless, there are some applications where this

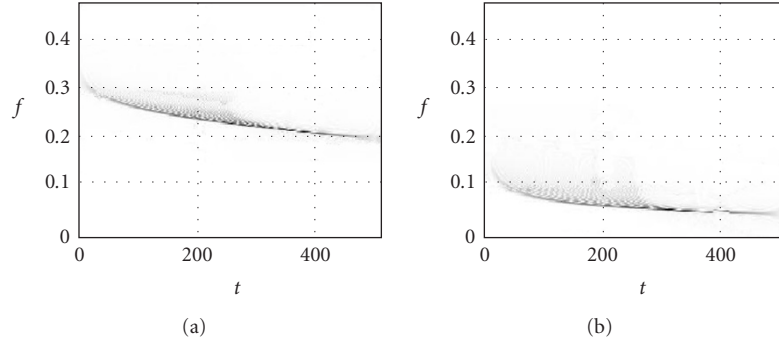


FIGURE 5: WVD of (a) original signal ( $\text{WVD}_s(t, f)$ ) and (b) warped signals in conventional time-frequency coordinates ( $\text{WVD}_{U_{1/K}s}(t, f)$ ).

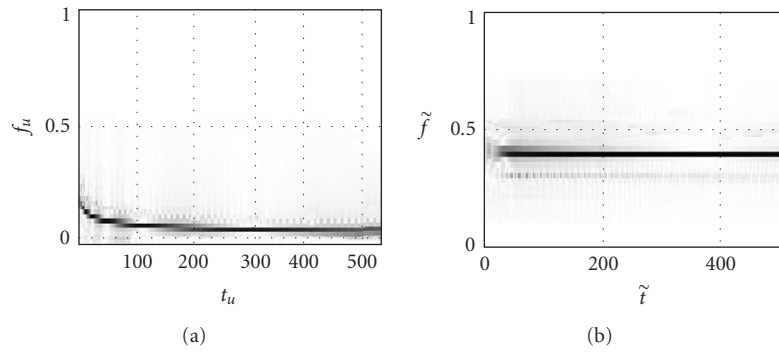


FIGURE 6: The effect of the warping operator in new time-frequency plane. (a)  $\text{WVD}_{U_{1/K}s_u}(t_u, f_u)$ . (b)  $\text{WVD}_{U_{1/K}s_u}(\tilde{t}, \tilde{f})$ .

information is not available (passive sonar and radar fields, recognition of digital modulations, etc.). In order to deal with these situations, many methods have been developed [18, 19]. The common used technique is the signal decomposition on an extended dictionary composed of elementary functions with nonlinear time-frequency behavior. After the signal decomposition with such dictionary, the extracted elementary functions are optimally represented in a time-frequency plane, using the associated warping operators. These methods, which constitute the generalization of the chirplet-transform-based methods [20], are often limited in practical applications by a required huge dictionary size.

An alternative to characterize the nonlinear time-frequency behavior of an unknown signal is described in the next section. This method is based on the polynomial phase modeling associated with a new polynomial phase removing procedure. The objective is to reduce the error propagation effect described in Section 3. Conceptually, a warping operator is designed to replace the polynomial order reduction stage described in relation (9). This warping operator is generally defined as

$$U_k : w_k(t) = \left( \frac{t}{\hat{a}_k} \right)^{1/k}, \quad (37)$$

where  $\hat{a}_k$  is the estimation of the  $k$ th-order polynomial coefficient. The following example illustrates the effect of this

warping operator for a 3rd-order PPS given by

$$s(t) = e^{j2\pi(0.37t - 4.6 \cdot 10^{-4} \cdot t^2 + 3 \cdot 10^{-6} \cdot t^3)} \quad (38)$$

whose WVD is plotted in Figure 7a.

Applying the warping operator (37) (for  $k = 3$  and  $\hat{a}_3$  close to the real value  $a_3$ ) to the oversampled version of the signal (38), we obtain the warped signal

$$\begin{aligned} (U_3 s_u)(t_u) &\approx e^{j2\pi[0.37(t_u/\hat{a}_3)^{1/3} - 4.6 \cdot 10^{-4}(t_u/\hat{a}_3)^{2/3} + t_u]} \\ &= e^{j2\pi[0.37(t_u/\hat{a}_3)^{1/3} - 4.6 \cdot 10^{-4}(t_u/\hat{a}_3)^{2/3}]}. e^{j2\pi t_u}, \end{aligned} \quad (39)$$

where  $t_u$  is the time axis issued after oversampling ( $u = 10$ ).

As shown in [17] and practically illustrated in the example previously presented, the effect of the time-frequency content linearization provided by a general warping operator is “visible” by the evaluation of the WVD for new time-frequency coordinates.

Alternatively, if the warping operator is designed to reduce the polynomial order of a signal, its effect will be depicted by computing the HIM corresponding to the new polynomial order. Knowing that the 2nd-order HIM is the classical instantaneous correlation function which appears in the WVD definition [16], the effect of 2nd-order HIM application is equivalent to the evaluation of the WVD. For this reason, we illustrate, in Figure 7c, the WVD of that signal (39). We remark that a linear time-frequency structure was generated. This result explains, for the example considered

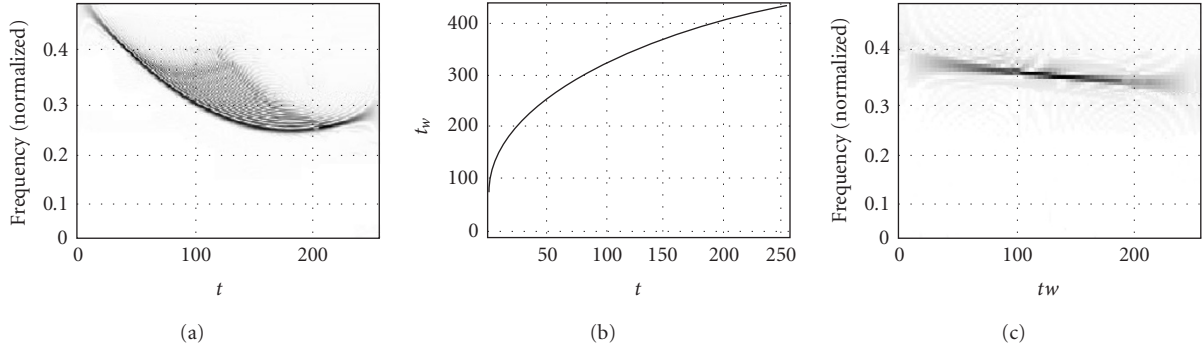


FIGURE 7: Polynomial order reduction using the warping operator (37). (a) WVD of original signal. (b) Warping law. (c) WVD of warped signal.

above, that the warping operator defined by (37) has, in association with the corresponding HIM, an order-reducing effect.

Applying the warping procedure described in Figure 4, some artifacts appear in practice (Figure 7c). They are caused by the errors induced by numerical computations. As illustrated in these figures, these artifacts are not disturbing since the main linear time-frequency component is much more energetic. However, these errors might be reduced by increasing the oversampling rate  $u$  [17]. Nevertheless, from computational tractability point of view, this rate cannot be arbitrarily high. In the case of the warping operator defined by the expression (37), the method for the evaluation of the value of oversampling parameter  $u$  is described in the appendix.

The polynomial order removing of the warping operator defined in (27) is used in the following section. Also, we will prove, in a more rigorous manner, that it is possible to successively reduce the order of the phase modeling by iterative applications of this warping operator.

## 5. WARPED-BASED POLYNOMIAL ORDER REDUCTION

In this section, we will mathematically prove the property of the warping operator (37) to reduce the polynomial order of the signal.

We consider an  $N$ th-order PPS defined by the relation (1). Using a modern version of the HAF-based polynomial modeling procedure (PHAF operator or the approach proposed in [11]), we can obtain an accurate estimate of the  $N$ th-order polynomial coefficient, denoted by  $\hat{a}_N$ . With this estimation, we design, via (37), the corresponding warping operator:

$$w_N : t \xrightarrow{U_N} t_w^{(N)} = w_N(t) = \left( \frac{t}{|\hat{a}_N|} \right)^{1/N}. \quad (40)$$

Some implementation issues associated to this warping operator are commented in the appendix. Mathematically, the effect of the associated unitary operator  $U$  on the PPS

is depicted, in the new time coordinate, as

$$\begin{aligned} & (\mathbf{U}_N s)(t_w^{(N)}) \\ &= \tilde{A} \exp \left\{ j a_N \left[ \left( \frac{t}{|\hat{a}_N|} \right)^{1/N} \right]^N \right\} \cdot \exp \left\{ j \sum_{m=0}^{N-1} a_m [t_w^{(N)}]^m \right\} \\ &= \underbrace{\tilde{A} \exp \left\{ j \sum_{m=0}^{N-1} a_m [t_w^{(N)}]^m \right\}}_{(N-1)\text{th-order PPS}(s^{(N-1)})} \cdot \underbrace{\exp \left\{ j \frac{a_N}{|\hat{a}_N|} t \right\}}_{\text{residual } r(t)}, \end{aligned} \quad (41)$$

where

$$\tilde{A} = A \sqrt{\frac{1}{N |\hat{a}_N|} \left( \frac{t}{|\hat{a}_N|} \right)^{1/N-1}}. \quad (42)$$

Since all the terms in (42) are known and nonrandom, the induced amplitude modulation can be compensated, for example, through an amplitude weighting using the inverse of relation (42).

Therefore, the result of the warping transform of an  $N$ th-order PPS consists in a  $(K-1)$ th-order PPS with a new temporal variable  $t_w^{(N)}$ . The  $(N-1)$ th-order PHAF of this signal, with respect to the variable  $t_w^{(N)}$ , peaks to a frequency location related, via relation (6), to the  $a_{N-1}$  coefficient. To prove that, we compute the  $(N-1)$ th-order HIM of the  $\mathbf{U}_N s$  signal:

$$\begin{aligned} & \text{HIM}_{N-1} [\mathbf{U}_N s^{(N)}; \tau] \\ &= \text{HIM}_{N-1} [s^{(N-1)}(t_w^{(N)}); \tau] \cdot \text{HIM}_{N-1} [r(t); \tau]. \end{aligned} \quad (43)$$

The first term of the product (43) is a sinusoid associated to the  $(N-1)$ th-order polynomial coefficient:

$$\text{HIM}_{N-1} [s^{(N-1)}(t_w^{(N)}); \tau] = A^{2^{N-2}} e^{j(N-1)a_{N-1}\tau^{N-2}t_w^{(N)}} \quad (44)$$

because it represents the  $(N-1)$ th-order HIM of the  $(N-1)$ th-order PPS which appears in (41).

From property (4), it is easy to show that the second term of (41) is 1 for  $N > 2$ :

$$\begin{aligned} \text{HIM}_2[r(t); \tau] &= e^{j(a_N/\hat{a}_N)t} \cdot e^{-j(a_N/\hat{a}_N)(t-\tau)} = e^{j(a_N/\hat{a}_N)\tau}, \\ \text{HIM}_3[r(t); \tau] &= e^{j(a_N/\hat{a}_N)\tau} \cdot e^{-j(a_N/\hat{a}_N)\tau} = 1, \\ &\vdots \\ \text{HIM}_N[r(t); \tau] &= 1 \cdot 1 = 1, \quad N \geq 3. \end{aligned} \quad (45)$$

Consequently, the  $(N - 1)$ th-order HIM of the  $\mathbf{U}_N s$  signal is

$$\text{HIM}_{N-1}[\mathbf{U}_N s^{(N)}; \tau] \left( t_w^{(N)} \right) = A^{2^{N-2}} e^{j(N-1)! a_{N-1} \tau^{N-2} t_w^{(N)}}. \quad (46)$$

As stated by this relation, for  $N > 2$ , the  $(N - 1)$ th-order HIM of the warped signal  $\mathbf{U}_N s$  does not contain any term related to the residual  $r$  given by (41). Consequently, the estimated value of the  $N$ th-order coefficient does not act in the estimation procedure of the  $(N - 1)$ th order. Actually, from a theoretical point of view, we could eliminate the  $|\hat{a}_N|$  from the structure of the warping operator defined in (40). In this case, we should have obtained the same results as in (45): the  $N$ th-order HIM of  $r(t)$  is 1 for  $N > 2$ . This proves the independence of the estimation procedure at a given order on the coefficients already estimated.

Hence, as shown in the appendix, the presence of  $|\hat{a}_N|$  in the definition of the warping operator (40) is dictated by practical reasons: the necessary values of the oversampling rate will have a reasonable value.

Then, we use the PHAF-based method to estimate the coefficient  $a_{N-1}$ . Via (37), with this new value we construct a new warping operator used to reduce the  $(N - 1)$ th order as described in (41).

This procedure is iterated until all polynomial coefficients are estimated. Practically, the new polynomial estimation method is depicted in the block diagram (Figure 8).

Unlike the classical order reduction technique (relation (9)), the warping-based order reduction eliminates from the expression of the warped signal the terms related to the estimation at the higher orders. In consequence, as it is theoretically proved by the relations (41) and (46), the performances of the PHAF-based estimation procedure theoretically depend *only* on the result at the given order. This fact, proved by relations (43), (44), (45), and (46), constitutes the main important feature of the warping operator (40) and its use for order reduction (41).

However, as the error analysis (provided through simulations) will prove in the next section, the estimation error at a given order is practically independent of the errors which occur for higher orders.

## 6. SIMULATION RESULTS

To demonstrate the capabilities of the warping-based order reduction, some simulation results will be presented. The method proposed in the previous section will be compared with the conventional PHAF (i.e., the polynomial order reduction is done by the classical procedure depicted in (9)).

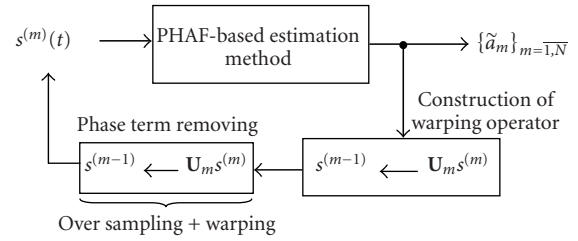


FIGURE 8: Polynomial coefficient estimation based on warping phase order removing.

Since the PHAF performing for a polynomial order larger than 3 is influenced by the error propagation effect, we limit our simulations to the third order. However, as shown in Section 3, the error propagation effect becomes “visible” after three iterations. Consequently, the choice of third-order phase modeling in our simulation should be enough to objectively compare the second-order reducing procedures.

The performances of this new approach are firstly proved in terms of estimation error variances as a function of the SNR. We assumed a 3rd-order PPS, given by the relation (38), embedded in white Gaussian noise. Two methods have been compared—PHAF-based estimation method and PHAF-based estimation method with warping-based phase compensation (denoted by “WarpComp” method). Each variance was computed for 500 trials and, for each order, it was compared with the Cramer-Rao bound (CRB) evaluated in [21].

The first plot proves that, for the highest-order, the performances of both methods are similar: the estimation of the highest-order coefficient (a3) depends on the noise level. The next two pictures show that, using the warping-based phase compensation, the estimation performances remain close to the CRB as in the case of the highest-order coefficient. Consequently, the performances of this method depend only on the noise, whereas in the PHAF case they are affected also by the error propagation phenomenon.

The statistical analysis provided by the Figure 9 shows clearly the reduction of the error propagation effect which acts in the case of the classical phase order compensation (relation (9)).

The cancellation of the error propagation effect is also illustrated in Figure 10, using the signal proposed in (14).

The estimated values of the polynomial coefficients and of the PHAF peaks are depicted in Table 2.

As the figure shows, the proposed method for polynomial order reduction provides a much more accurate estimation of the IFL than methods which use the classical phase order reduction (for comparison see Figure 3).

As pictured in the PHAF subplots at each order, the dependence between the errors occurred at these orders is practically eliminated: there is a single prominent peak corresponding to the polynomial coefficients. No spurious peaks, independent of the considered order (Figure 10a), are identified. Accordingly, these coefficients are accurately estimated with respect to the real one (26). Therefore, the polynomial

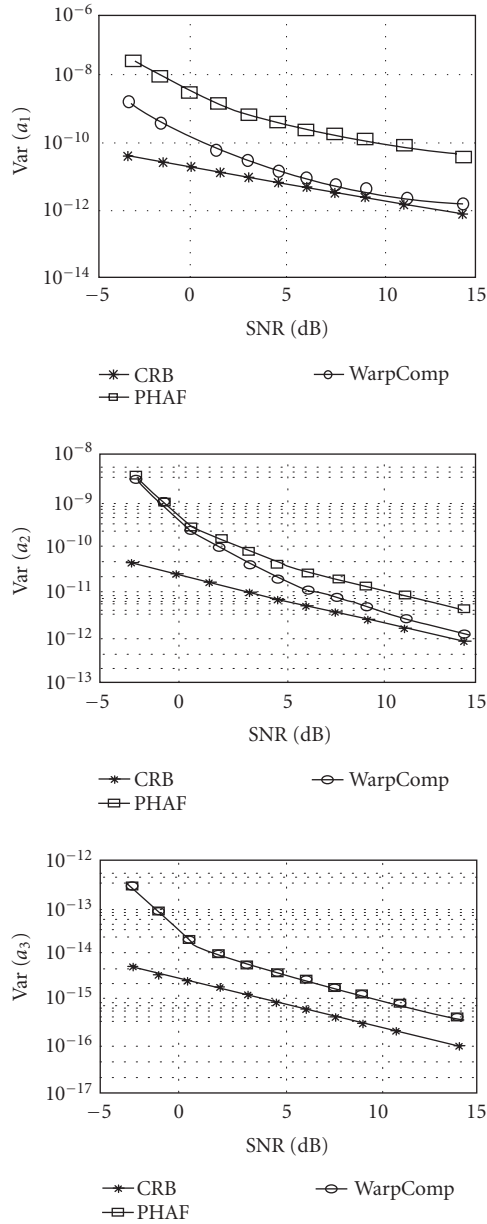


FIGURE 9: The estimated variances versus SNR.

order reduction through the procedure based on the warping operators improves considerably the performances of the PHAF-based estimation procedure.

This property is also pointed up in Figure 11, in the case of some signals of different types: sinusoidal frequency modulation (SFM) (Figure 11a), a signal emitted by a Diesel engine [23] (Figure 11b), and a signal received from an underwater mobile emitting a chirp (Figure 11c).

For each of those signal types, we note that the polynomial approximations provided by the proposed approach are correctly related to the theoretical IFL or with the information provided by a classical method (spectrogram). In the case of the signal emitted by a Diesel engine (Figure 11b), the polynomial phase approximation provided by the proposed

approach is expressed as

$$\begin{aligned} \phi(t) = & 539 \cdot t + 2.32 \cdot 10^{-2} \cdot t^2 - 1.32 \cdot 10^{-6} \cdot t^3 \\ & + 3.67 \cdot 10^{-11} \cdot t^4 - 5.4 \cdot 10^{-16} \cdot t^5. \end{aligned} \tag{47}$$

In Figure 11c, we analyze the signal received from an underwater moving source (having a velocity  $v = 6$  m/s and an acceleration  $a = 0.07$  m/s<sup>2</sup>; the source moves away from the receiver). We supposed that the source transmits a chirp given by  $\exp[j2\pi(410t + 2.48t^2)]$  and the receiver sampling frequency is  $F_s = 1000$  Hz. In this configuration, as shown in [24], received signal phase becomes a fourth-order polynomial. Its estimation, provided by the method proposed in this paper, is given by

$$\begin{aligned} \phi(t) = & 0.41 \cdot t + 3.82 \cdot 10^{-4} \cdot t^2 \\ & - 3.15 \cdot 10^{-6} \cdot t^3 + 1.63 \cdot 10^{-9} \cdot t^4. \end{aligned} \tag{48}$$

Its representation is illustrated in Figure 11c. Using the estimated values of the polynomial coefficients (relation (48)) we can evaluate the motion parameters [24].

As illustrated by these examples, the warped-based phase modeling provides a high-order polynomial parametric information about the analyzed process which consists in a set of polynomial coefficients. This information could be used in various applications such as modulation recognition process, machinery diagnostic, or motion tracking [24].

The following example shows the capability of the proposed approach to deal with multicomponent real signals. As a test signal we have considered an emission of an underwater mammal (*Tursiops Marineland*) (see Figure 12) [22].

The IFLs of the time-frequency components of the analyzed signal are superposed on the spectrogram of this signal. Two remarks can be made. Firstly, the approximation shapes given by the polynomial modeling are characterized by an improved resolution with respect to the spectrogram one. Secondly, the analytical description of the time-frequency content offers useful information about the studied process.

These results have been obtained for an assumed highest polynomial order. Nevertheless, in practice, this assumption, based on a priori information, is often inappropriate to the studied processes. Two cases could be devised.

In the first case, the estimation of the highest order of polynomial approximation is directly related to the analyzed processes. For example, in the case of an underwater mobile emitting a chirp, a second-order motion law (characterized by a velocity and an acceleration) transforms the received signal in a fourth-order PPS [19]. It is the case of the signal studied in Figure 11c where the fourth-order warping-based phase modeling provides the information about the motion law.

In the second case, if the analyzed processes cannot be the subject of any physical assumption or the signal cannot be assimilated to a PPS, the choice of the highest order is often accomplished after many tries and a postprocessing analysis.

Generally, the choice is based on a tradeoff between the accuracy of the IFL estimation and the artifacts induced by

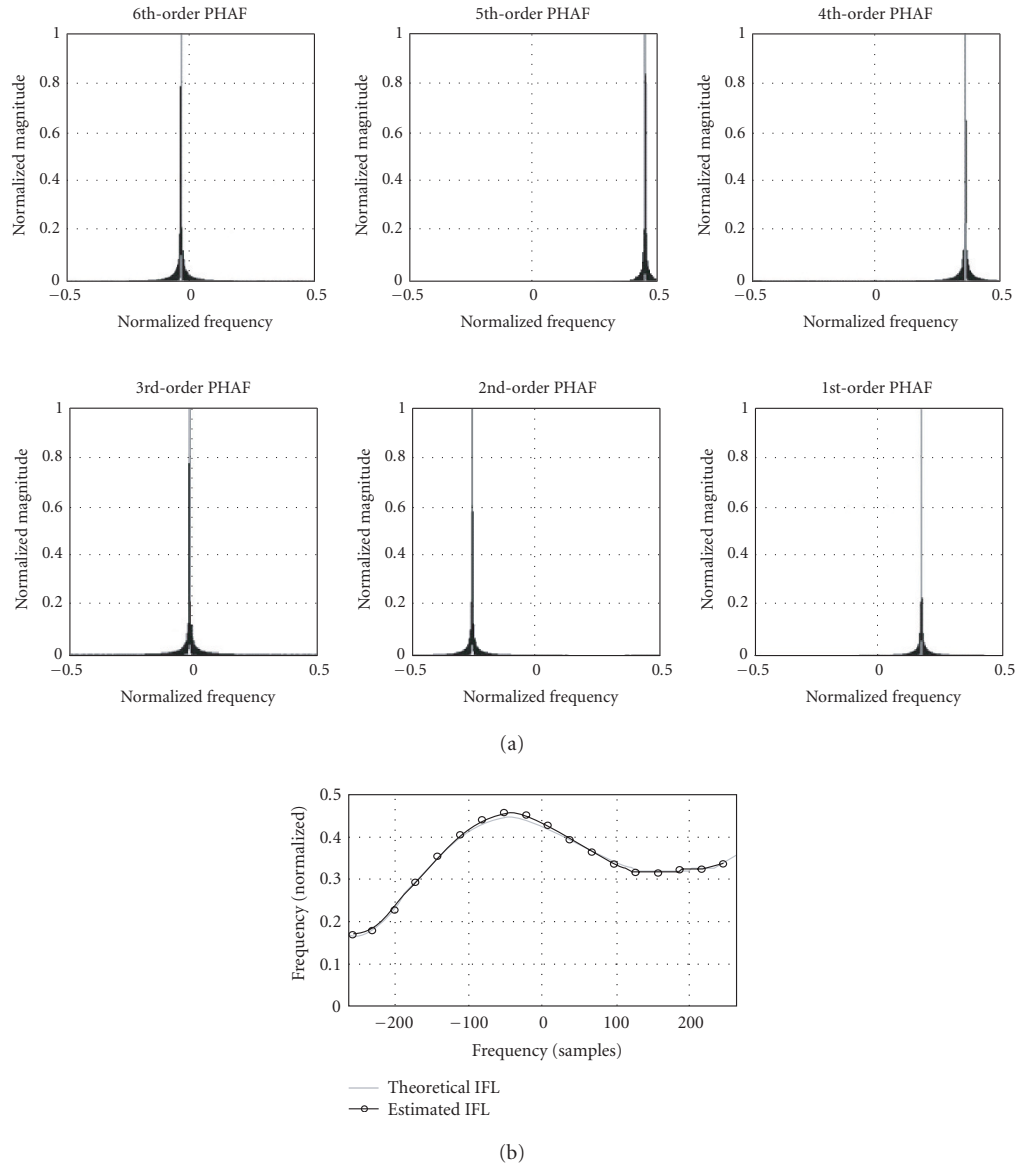


FIGURE 10: PHAF-based phase modeling using warping order reduction. (a) Warped-based phase removing. (b) Theoretical and estimated IFL.

TABLE 2: Polynomial coefficients estimated by PHAF using warping order reduction.

	$\hat{\alpha}_1$	$\hat{\alpha}_2$	$\hat{\alpha}_3$	$\hat{\alpha}_4$	$\hat{\alpha}_5$	$\hat{\alpha}_6$
Values	0.1719	-0.2987	-0.0147	0.381	0.4714	-0.0817
	$\hat{a}_1$	$\hat{a}_2$	$\hat{a}_3$	$\hat{a}_4$	$\hat{a}_5$	$\hat{a}_6$
Values	0.1719	$-9.762 \cdot 10^{-4}$	$-2.36 \cdot 10^{-7}$	$3.798 \cdot 10^{-8}$	$2.8 \cdot 10^{-10}$	$-3.29 \cdot 10^{-13}$

an order higher than a real one. To illustrate this tradeoff, we consider the high-order warping modeling of the signal defined in (26), embedded in a white Gaussian noise (SNR = 10 dB).

If the approximation order is 4, inferior to the real one ( $N = 6$ ), the 5th- and 6th-order coefficients are ignored. Consequently, the estimated IFL does not contain all the real

IFL details (Figure 13a). Alternatively, if the approximation order is superior to 6 (Figure 13b), the estimation of the 7th- and 8th orders is strongly affected by the noise. More precisely, since the 6th-order PPS is noise corrupted, the estimations of 7th- and 8th-order coefficients are given by the spectral peaks associated to the noise. These ones are plotted in Figure 14.

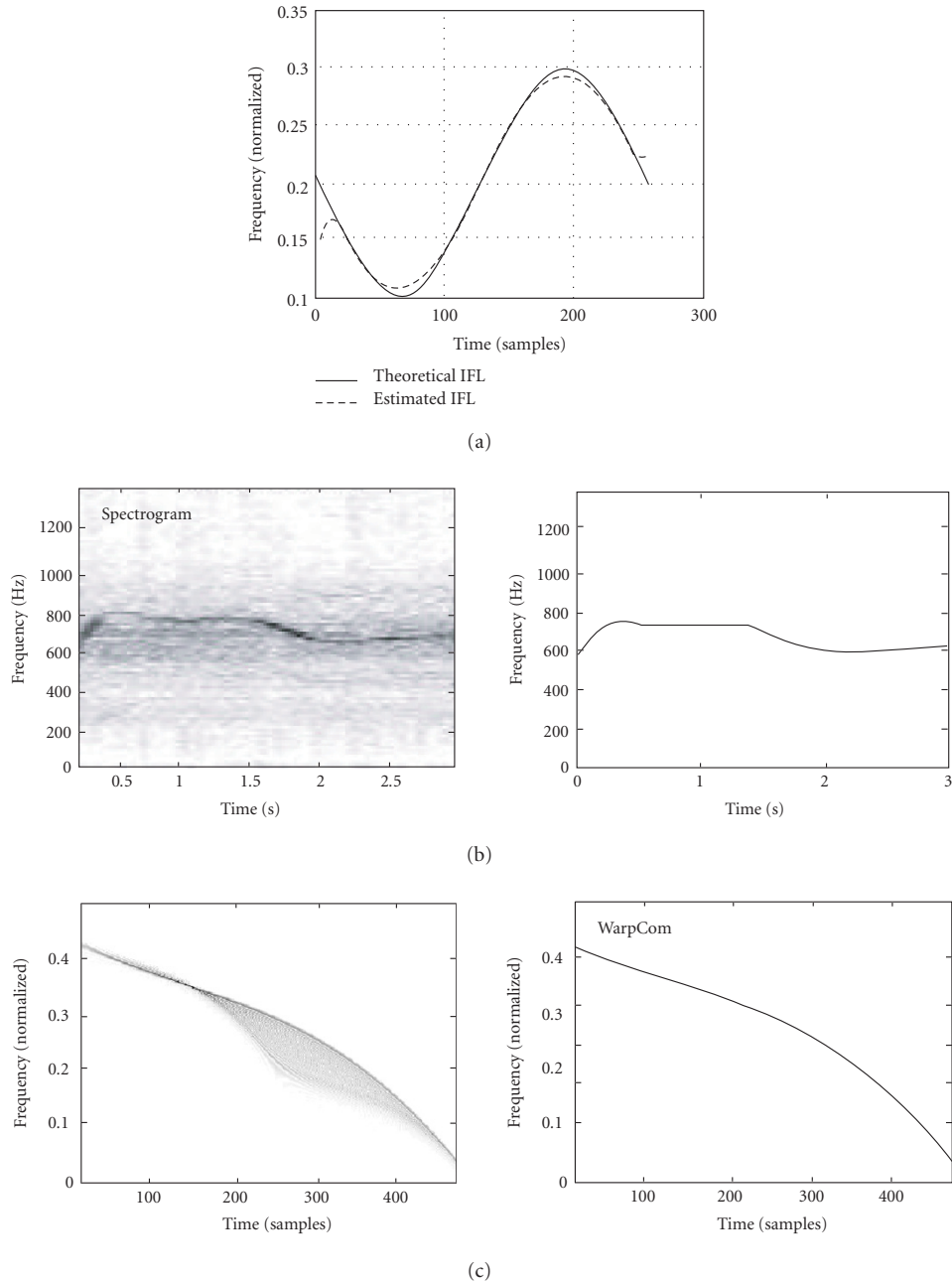


FIGURE 11: Several signal-type characterizations by warped-based high-order phase modeling. (a) SFM characterization via WarpComp. (b) Characterization, via WarpComp, of a diesel engine sound. (c) Characterization, via WarpComp, of a received signal from a moving target.

The estimated values of the polynomial coefficients are given in Table 3.

These coefficients, which ideally (noise free signal) should be 0, have nonzero values as indicated in Figure 14. Using the proposed approach, these nonzero values do not affect the lower-order estimations. This is proved by the position of PHAFs peaks which are almost similar to the ones obtained when the correct highest order has been used (see Figure 10). Nevertheless, the 7th and 8th polynomial coefficients introduce some artifacts in the IFL structure (Figure 13b).

In practice, the problem becomes more difficult since the signal is not analytical (its phase cannot be expressed in a polynomial form). However, since the general purpose of the polynomial phase modeling is to provide a more detailed and accurate description of the time-frequency content, an arbitrary order, even if it is not the “optimal” one, gives better results than the conventional methods (Cohen’s class, warping-based TFRs, etc.) do.

The proposed method (warping-based phase modeling) allows, by reducing the error propagation effect, to increase the highest polynomial order of the classical procedures for

TABLE 3: Polynomial coefficients estimated by PHAF using warping order reduction.

	$\hat{\alpha}_1$	$\hat{\alpha}_2$	$\hat{\alpha}_3$	$\hat{\alpha}_4$	$\hat{\alpha}_5$	$\hat{\alpha}_6$	$\hat{\alpha}_7$	$\hat{\alpha}_8$
Values	0.1719	-0.2987	-0.0147	0.381	0.4714	-0.0817	0.0355	0.0493
	$\hat{a}_1$	$\hat{a}_2$	$\hat{a}_3$	$\hat{a}_4$	$\hat{a}_5$	$\hat{a}_6$	$\hat{a}_7$	$\hat{a}_8$
Values	0.1719	$-9.762 \cdot 10^{-4}$	$-2.36 \cdot 10^{-7}$	$3.798 \cdot 10^{-8}$	$2.8 \cdot 10^{-10}$	$-3.29 \cdot 10^{-13}$	$1.01 \cdot 10^{-15}$	$1.02 \cdot 10^{-17}$

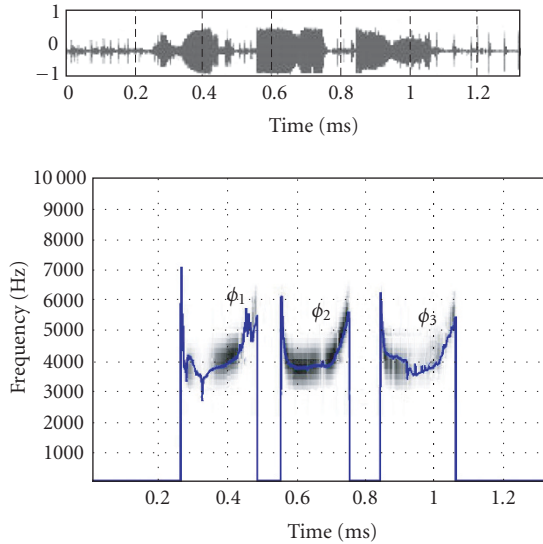


FIGURE 12: Polynomial phase modeling of an underwater signal using the warped-based order reduction.  $\phi_1(t) = 7105 \cdot t - 2.69 \cdot t^2 + 7.619 \cdot 10^{-4} \cdot t^3 - 8.21 \cdot 10^{-8} \cdot t^4$ ;  $\phi_2(t) = 6050 \cdot t - 3.68 \cdot t^2 + 14 \cdot 10^{-4} \cdot t^3 - 2.26 \cdot 10^{-7} \cdot t^4$ ; and  $\phi_3(t) = 6250 \cdot t - 1.77 \cdot t^2 + 4.4 \cdot 10^{-4} \cdot t^3 - 5.6 \cdot 10^{-8} \cdot t^4$ .

polynomial phase modeling. As illustrated in the previous examples, this property leads naturally to an improved time-frequency analysis of the signal.

## 7. CONCLUSION AND FUTURE WORK

In this paper we proposed a new method for polynomial order reduction, based on the axis warping principle, applied to each polynomial order. This method constitutes an attractive way to attenuate the effect of error propagation which inherently appears in any PPS estimation algorithm. Actually, the involved warping operator is designed to reduce, in association with the HIM evaluated for the current order, the phase order of the signal as illustrated in Section 4. Thence, its iterative application associated with a modern polynomial estimation method (e.g., PHAF) guarantees good results for the polynomial modeling procedure.

Conceptually speaking, the proposed technique is an alternative to the conventional tandem warping operator and bilinear time-frequency distribution. Since the last one is devised to linearize the time-frequency content of the signal, the new warping operator structure and the HIMs provide a new way for polynomial coefficient estimation. In this context, the main property is the reduction of the error influence between the polynomial orders.

In practical terms, the performing of this combination does not involve the knowledge about the nature of the signal as the classical warping operators do. Assuming a polynomial phase model, which is generally for a large class of signals, the phase modeling is done by applying iteratively an order-depending warping operator and the main tool for polynomial coefficient estimation, the HIM.

The statistical analysis and the several examples prove that this method can be successfully used to estimate the polynomial model of a general class of signals. Transitory signals, digital modulations, and speech are only some examples of signals whose polynomial phase modeling demands a high polynomial order. Consequently, the proposed method represents a potential solution to deal with these signals. As demonstrated by the results, this method, associated with a modern procedure of polynomial coefficient estimation (e.g., PHAF) gives accurate time-frequency information about the analyzed signal. The examples of real signals show the potential of the proposed approach to manage with real-life signals.

In further works, assuming a polynomial model of the signal, we will try to define its *generalized* warping operator as the mathematical composition of the particular operators defined for each polynomial order.

On the other hand, since the “optimal” highest order seems to be depending on the time-frequency structure of the signal, we intend to study some criteria to establish, in a given context (application and signal type), the most appropriate highest order. For example, one of the criteria could be the correlation between the real signal and the synthesized one from the estimated polynomial coefficients.

In the application field, the development of a signal classification and identification system, based on the proposed approach, will be investigated. In the configuration, this method can be used as a feature extraction stage. The information concerning different signals is provided by the polynomial coefficients issued by estimation. Based on the richness of the information given by these coefficients, we can separate two signals with a close time-frequency behavior. As a practical application, we intend to apply this feature extraction method in the passive oceanic acoustic tomography [19]. The particularity of this application—signals emitted by marine mammals— involves the use of a method able to provide an accurate characterization of these signals. Knowing that these signals have generally a nonlinear time-frequency behavior, the method proposed in this paper constitutes a potential solution in the context of the passive oceanic acoustic tomography.

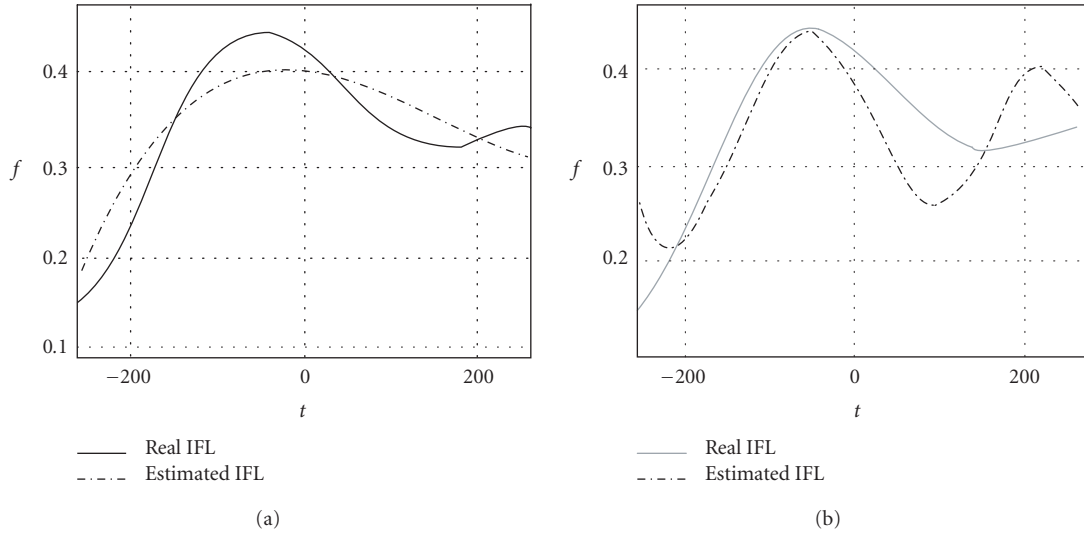


FIGURE 13: Influence of the choice of the highest polynomial order. (a) Fourth-order phase modeling. (b) Eighth-order phase modeling.

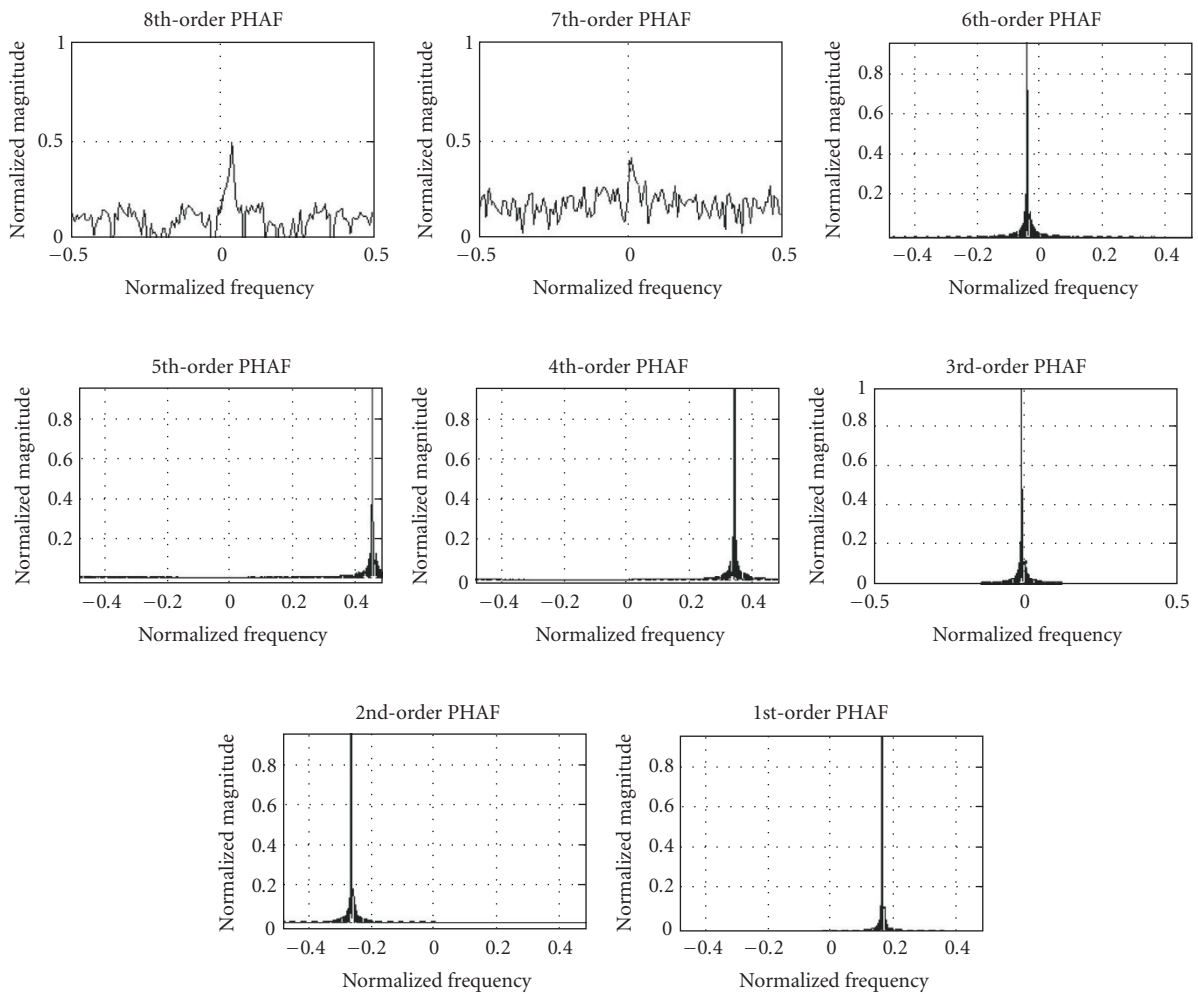


FIGURE 14: Noise influence on the polynomial phase modeling via WarpCom using an overestimated polynomial order (8 instead of 6).

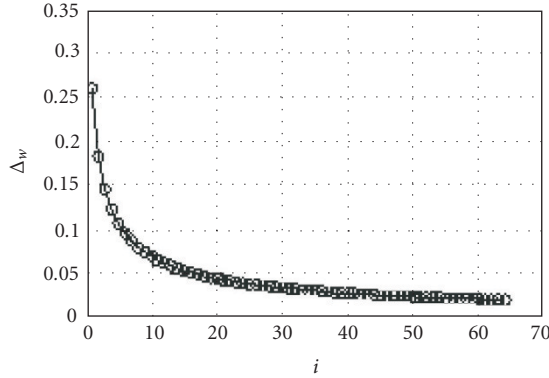


FIGURE 15: Values of the distances between two consecutive points of warped time axis.

## APPENDIX

### CONSIDERATIONS ON COMPUTATIONAL ISSUES

In this section some implementation details are treated to demonstrate several claims included in this paper. First, we demonstrate the motivation for the warping operator defined in (40) giving also a method for choosing the oversampling rate at each order.

We consider firstly the warping operator defined by (33). Its discrete version can be written as

$$w[i] = (i\Delta)^{1/k}, \quad k \geq 1, \quad i = 1, \dots, L, \quad (\text{A.1})$$

where  $\Delta$  is the sampling rate of the original signal  $x$  and  $L$  is the number of samples. According to this expression, the points of the new time axis,  $t_w$ , produced by this operator will be nonuniformly spaced. The distances between two consecutive points,  $\Delta_w$ , are given by

$$\begin{aligned} \Delta_w[i] &= w[i+1] - w[i] = [(i+1)\Delta]^{1/k} - (i\Delta)^{1/k} \\ &= [(i+1)^{1/k} - i^{1/k}] \Delta^{1/k}, \quad i = 1, \dots, L-1. \end{aligned} \quad (\text{A.2})$$

For an initial sampling rate  $\Delta = 1$  and  $L = 64$  samples, the values of  $\Delta_w$  provided by the warping operator (A.1) of order 3 are plotted in Figure 15.

As proved by (A.2) and illustrated in Figure 15, the differences between the points of warped axes  $t_w$  are inferior to the initial sampling rate  $\Delta$ . Consequently, by using the original sampling rate, the samples of the warped signal cannot be evaluated for these points. This can be solved by considering an oversampling procedure before the evaluation of the warped signal samples (as indicated in Figure 4). The value of oversampling rate  $u$  must be sufficiently high to ensure the evaluation of warped signal for all new time coordinates. Mathematically, this condition can be written as

$$\frac{\Delta}{u} \leq \min_{1 \leq i \leq L-1} \{\Delta_w[i]\}. \quad (\text{A.3})$$

This condition, mentioned in [17], states that points generated by oversampling of rate  $u$  are closer than the

minimum of the sampling rate requested by the new warped axis. This ensures that all the warped time coordinates will be taken into account.

With the observation that the minima of the  $\Delta_w[i]$  is obtained for  $i = L - 1$ , a general method for the choice of  $u$  is expressed as

$$u \geq \frac{\Delta^{1-1/k}}{[L^{1/k} - (L-1)^{1/k}]}. \quad (\text{A.4})$$

The expression (A.4) introduces an inferior limit for the oversampling rate. To avoid situations when a large value of  $u$  affects the computational performances of the machine, we set  $u$  as this bound.

Furthermore, samples of the warped signal  $x_w$  are obtained from samples of the oversampled signal  $\tilde{x}$  by a linear interpolation procedure, used also in [17]:

$$x_w(w[i]) = \tilde{x}(i\Delta_u) + [\tilde{x}((i+1)\Delta_u) - \tilde{x}(i\Delta_u)](w[i] - i\Delta_u), \quad (\text{A.5})$$

where  $\Delta_u = \Delta/u$  is the new sampling rate.

*Remark 1.* We consider the example considered in Figure 7:  $k = 3$ ,  $L = 256$ , and  $\Delta = 1$ . According to (A.4), the sufficient value for the  $u$  should be larger than 121. In order to avoid the increasing of signal length with a such large value, the idea, we adopted, consists in introducing the associated polynomial coefficient  $a_k$  in the structure of the warping operator as follows:

$$w[i] = \left( \frac{i\Delta}{|\hat{a}_k|} \right)^{1/k}, \quad k \geq 1, \quad i = 1, \dots, L. \quad (\text{A.6})$$

Namely, since the value of  $a_k$  is superiorly limited by  $\pi/k! \Delta (\Delta\tau)^{k-1}$  ( $\tau$  lag used for HIM computation) (condition imposed by a Nyquist-like depicted in [1, page 398]), the inferior borne of  $u$ ,

$$u \geq \frac{1}{[L^{1/k} - (L-1)^{1/k}]} \left( \frac{\Delta}{|\hat{a}_k|} \right)^{1-1/k}, \quad (\text{A.7})$$

decreases through a more reliable value from the computational point of view.

For the previous example ( $a_3 = 2 \cdot 10^{-6}$ ), the new value of  $u$  is about 20.

In conclusion, the presence of  $\hat{a}_k$  in the warping operator structure defined in (40) is justified by practical considerations: the complexity remains reasonable in spite of signal length or phase order.

According to this new definition, it is easy to show that the value of  $u$  at the polynomial order  $k$  can be computed as

$$u^{(k)} = \frac{1}{[L^{1/k} - (L-1)^{1/k}]} \left( \frac{\Delta}{|\hat{a}_k|} \right)^{1-1/k}. \quad (\text{A.8})$$

## REFERENCES

- [1] B. Porat, *Digital Processing of Random Signals: Theory and Methods*, Prentice-Hall, Englewood Cliffs, NJ, USA, 1993.
- [2] S. Barbarossa, A. Scaglione, and G. B. Giannakis, "Product high-order ambiguity function for multicomponent polynomial-phase signal modeling," *IEEE Trans. Signal Processing*, vol. 46, no. 3, pp. 691–708, 1998.
- [3] B. Boashash and P. O'Shea, "Polynomial Wigner-Ville distributions and their relationship to time-varying higher order spectra," *IEEE Trans. Signal Processing*, vol. 42, no. 1, pp. 216–220, 1994.
- [4] L. J. Stankovic, "L-class of time-frequency distributions," *IEEE Signal Processing Lett.*, vol. 3, no. 1, pp. 22–25, 1996.
- [5] B. Porat and B. Friedlander, "Asymptotic statistical analysis of the high-order ambiguity function for parameter estimation of polynomial-phase signals," *IEEE Trans. Inform. Theory*, vol. 42, no. 3, pp. 995–1001, 1996.
- [6] S. Peleg, B. Porat, and B. Friedlander, "The achievable accuracy in estimating the instantaneous phase and frequency of a constant amplitude signal," *IEEE Trans. Signal Processing*, vol. 41, no. 6, pp. 2216–2224, 1993.
- [7] M. Benidir and A. Ouldali, "Polynomial phase signal analysis based on the polynomial derivatives decompositions," *IEEE Trans. Signal Processing*, vol. 47, no. 7, pp. 1954–1965, 1999.
- [8] C. Theys, M. Vieira, and A. Ferrari, "Bayesian estimation of the parameters of a polynomial phase signal using MCMC methods," in *Proc. IEEE International Conference on Acoustics, Speech and Signal Processing (ICASSP '97)*, vol. 5, pp. 3553–3556, Munich, Germany, April 1997.
- [9] G. T. Zhou and Y. Wang, "Exploring lag diversity in the high-order ambiguity function for polynomial phase signals," in *Proc. IEEE Signal Processing Workshop on Higher-Order Statistics (HOS '97)*, pp. 103–106, Banff, Alberta, Canada, July 1997.
- [10] R. G. Baraniuk and D. L. Jones, "Unitary equivalence: a new twist on signal processing," *IEEE Trans. Signal Processing*, vol. 43, no. 10, pp. 2269–2282, 1995.
- [11] C. Ioana and A. Quinquis, "High-order warped-based ambiguity function," in *Proc. IEEE-EURASIP Workshop on Nonlinear Signal and Image Processing (NSIP '03)*, Grado, Italy, June 2003.
- [12] S. M. Ruiz, "An algebraic identity leading to Wilson's theorem," *The Mathematical Gazette*, vol. 80, no. 489, pp. 579–582, 1996.
- [13] A. Papandreou, S. M. Kay, and G. F. Boudreaux-Bartels, "The use of hyperbolic time-frequency representations for optimum detection and parameter estimation of hyperbolic chirps," in *Proc. IEEE-SP International Symposium on Time-Frequency and Time-Scale Analysis (TFTS '94)*, pp. 369–372, Philadelphia, Pa, USA, October 1994.
- [14] F. Hlawatsch, A. Papandreou-Suppappola, and G. F. Boudreaux-Bartels, "The power classes-quadratic time-frequency representations with scale covariance and dispersive time-shift covariance," *IEEE Trans. Signal Processing*, vol. 47, no. 11, pp. 3067–3083, 1999.
- [15] T. Twaroch and F. Hlawatsch, "Modulation and warping operators in joint signal analysis," in *Proc. IEEE-SP International Symposium on Time-Frequency and Time-Scale Analysis (TFTS '98)*, pp. 9–12, Pittsburgh, Pa, USA, October 1998.
- [16] L. Cohen, *Time-Frequency Analysis*, Prentice-Hall, New York, NY, USA, 1994.
- [17] K. G. Canfield and D. L. Jones, "Implementing time-frequency representations for non-Cohen classes," in *Proc. 27th Asilomar Conference on Signals, Systems and Computers*, vol. 2, pp. 1464–1468, Pacific Grove, Calif, USA, November 1993.
- [18] A. Papandreou-Suppappola and S. B. Suppappola, "Adaptive time-frequency representations for multiple structures," in *Proc. 10th IEEE Workshop on Statistical Signal and Array Processing (SSAP '00)*, pp. 579–583, Pocono Manor, Pa, USA, August 2000.
- [19] R. G. Baraniuk and D. L. Jones, "Shear madness: new orthonormal bases and frames using chirp functions," *IEEE Trans. Signal Processing*, vol. 41, no. 12, pp. 3543–3549, 1993.
- [20] S. Mann and S. Haykin, "The chirplet transform: a generalisation of Gabor's logon transform," in *Proc. International Conference on Vision Interface (VI '91)*, pp. 205–212, Canadian Image Processing and Pattern Recognition Society, Calgary, Alberta, Canada, June 1991.
- [21] S. Peleg and B. Porat, "Estimation and classification of polynomial-phase signals," *IEEE Trans. Inform. Theory*, vol. 37, no. 2, pp. 422–430, 1991.
- [22] E. Delory and J. R. Potter, "Objectivity in the study of marine mammal vocalisations: a wavelet approach," in *Proc. 13th Annual Conference of European Cetacean Society (ECS '99)*, Valencia, Spain, April 1999.
- [23] <http://www.dolphinear.com/de-sound.htm>.
- [24] C. Ioana, A. Quinquis, C. Gervaise, and J.-C. Le Gac, "Motion estimation of underwater mobiles in a multipath channel using polynomial phase signal modelling," in *Proc. European Conference on Underwater Acoustic (ECUA '04)*, Delft, the Netherlands, July 2004.

---

**Cornel Ioana** received the Dipl.-Ing degree in electrical engineering and informatics in 1999 from the Romanian Military Technical Academy of Bucharest. Between 1999 and 2001 he acted as a military researcher in a research institute of the Romanian Ministry of Defense (METRA, Bucharest). He received the M.S. degree in telecommunication science in 2001 and the Ph.D. degree in the electrical engineering field in 2003, both from the University of Brest, France. Since 2003 he has worked as a researcher and development engineer in ENSIETA, Brest, France. His current research activity deals with the implementation of signal processing methods adapted to the passive underwater tomography. His technical interests are nonstationary signal processing, electronic warfare, sonar, and real-time systems.

**André Quinquis** received the M.S. degree in 1986 and the Ph.D. degree in 1989 in signal processing, both from the University of Brest. Between 1989 and 1992 he taught and developed research activities in signal and image processing at the Naval Academy in Brest. In 1992 he joined the Engineering School ENSIETA of Brest, where he held the positions of Senior Researcher and Head of the Electronics and Informatics Department. Since 2001 he has been the Scientific Director of ENSIETA. He is mainly interested in signal processing, time-frequency methods, and statistical estimation and decision theory. He is the author of 8 books and of more than 100 papers (international journals and conferences) in the area of signal processing.